

Probing the Structural Details of Chitin Nanocrystal–Water Interfaces by Three-Dimensional Atomic Force Microscopy

Ayhan Yurtsever,* Pei-Xi Wang, Fabio Priante, Ygor Morais Jaques, Kazuki Miyata, Mark J. MacLachlan, Adam S. Foster, and Takeshi Fukuma*

Chitin is one of the most abundant and renewable natural biopolymers. It exists in the form of crystalline microfibrils and is the basic structural building block of many biological materials. Its surface crystalline structure is yet to be reported at the molecular level. Herein, atomic force microscopy (AFM) in combination with molecular dynamics simulations reveals the molecular-scale structural details of the chitin nanocrystal (chitin NC)–water interface. High-resolution AFM images reveal the molecular details of chitin chain arrangements at the surfaces of individual chitin NCs, showing highly ordered, stable crystalline structures almost free of structural defects or disorder. 3D-AFM measurements with submolecular spatial resolution demonstrate that chitin NC surfaces interact strongly with interfacial water molecules creating stable, well-ordered hydration layers. Inhomogeneous encapsulation of the underlying chitin substrate by these hydration layers reflects the chitin NCs' multifaceted surface character with different chain arrangements and molecular packing. These findings provide important insights into chitin NC structures at the molecular level, which is critical for developing the properties of chitin-based nanomaterials. Furthermore, these results will contribute to a better understanding of the chemical and enzymatic hydrolysis of chitin and other native polysaccharides, which is also essential for the enzymatic conversion of biomass.

nanomaterials with improved functionalities.^[4,5] These nanomaterials have been successfully used as nano-fillers in nanocomposites, polymers, and thin films, leading to a reinforcement effect on the mechanical and thermal properties of the composite nanomaterials.^[6–9] Moreover, they have been suggested for water purification to remove heavy metals from contaminated water.^[10] They possess very active surfaces with abundant hydroxyl, hydroxymethyl, and acetamido side groups that can be suitably functionalized to use in drug delivery systems.^[11] In particular, recent studies have indicated that chitin-based nanocomposites have the potential to be employed as bioactive scaffolds for bone tissue engineering,^[12] enzyme/protein immobilization,^[13] biosensors,^[14–16] and battery separators.^[17]


Chitin is a naturally occurring linear biopolymer consisting of $\beta(1-4)$ linked *N*-acetyl-D-glucosamine residues as the building block of the chitin chain (as illustrated in **Figure 1a**), which can be commonly found in the shells of crustaceans, such as shrimps and crabs,^[18] and the cell walls of fungi. Chitin possesses many structural and functional similarities with cellulose. Like cellulose, it exists in nature as ordered crystalline microfibrils in association with some proteins and minerals.^[19] Pure chitin nanocrystals (NCs) can be generally obtained by a series of chemical and mechanical treatments of crab and shrimp shells to remove impurities.^[20] Chitin adopts three different crystalline polymorphs, namely, α -chitin, β -chitin, and γ -chitin, which

1. Introduction

Natural polysaccharide-based nanocrystals (including chitin and cellulose) derived from renewable natural resources have received considerable research attention in recent years.^[1–3] Their extraordinary mechanical and chemical properties, combined with their biodegradability, biocompatibility, and antimicrobial features, make them attractive for developing diverse

crabs,^[18] and the cell walls of fungi. Chitin possesses many structural and functional similarities with cellulose. Like cellulose, it exists in nature as ordered crystalline microfibrils in association with some proteins and minerals.^[19] Pure chitin nanocrystals (NCs) can be generally obtained by a series of chemical and mechanical treatments of crab and shrimp shells to remove impurities.^[20] Chitin adopts three different crystalline polymorphs, namely, α -chitin, β -chitin, and γ -chitin, which

A. Yurtsever, K. Miyata, M. J. MacLachlan, A. S. Foster, T. Fukuma
WPI Nano Life Science Institute (WPI-Nano LSI)
Kanazawa University
Kakuma-machi, Kanazawa 920-1192, Japan
E-mail: yurtsever@staff.kanazawa-u.ac.jp; fukuma@staff.kanazawa-u.ac.jp

 The ORCID identification number(s) for the author(s) of this article can be found under <https://doi.org/10.1002/smt.202200320>.

© 2022 The Authors. Small Methods published by Wiley-VCH GmbH. This is an open access article under the terms of the Creative Commons Attribution-NonCommercial License, which permits use, distribution and reproduction in any medium, provided the original work is properly cited and is not used for commercial purposes.

P.-X. Wang, M. J. MacLachlan
Department of Chemistry
University of British Columbia 2036 Main Mall
Vancouver V6T 1Z1, Canada

F. Priante, Y. Morais Jaques, A. S. Foster
Department of Applied Physics
Aalto University
FI-00076 Helsinki, Finland

DOI: 10.1002/smt.202200320

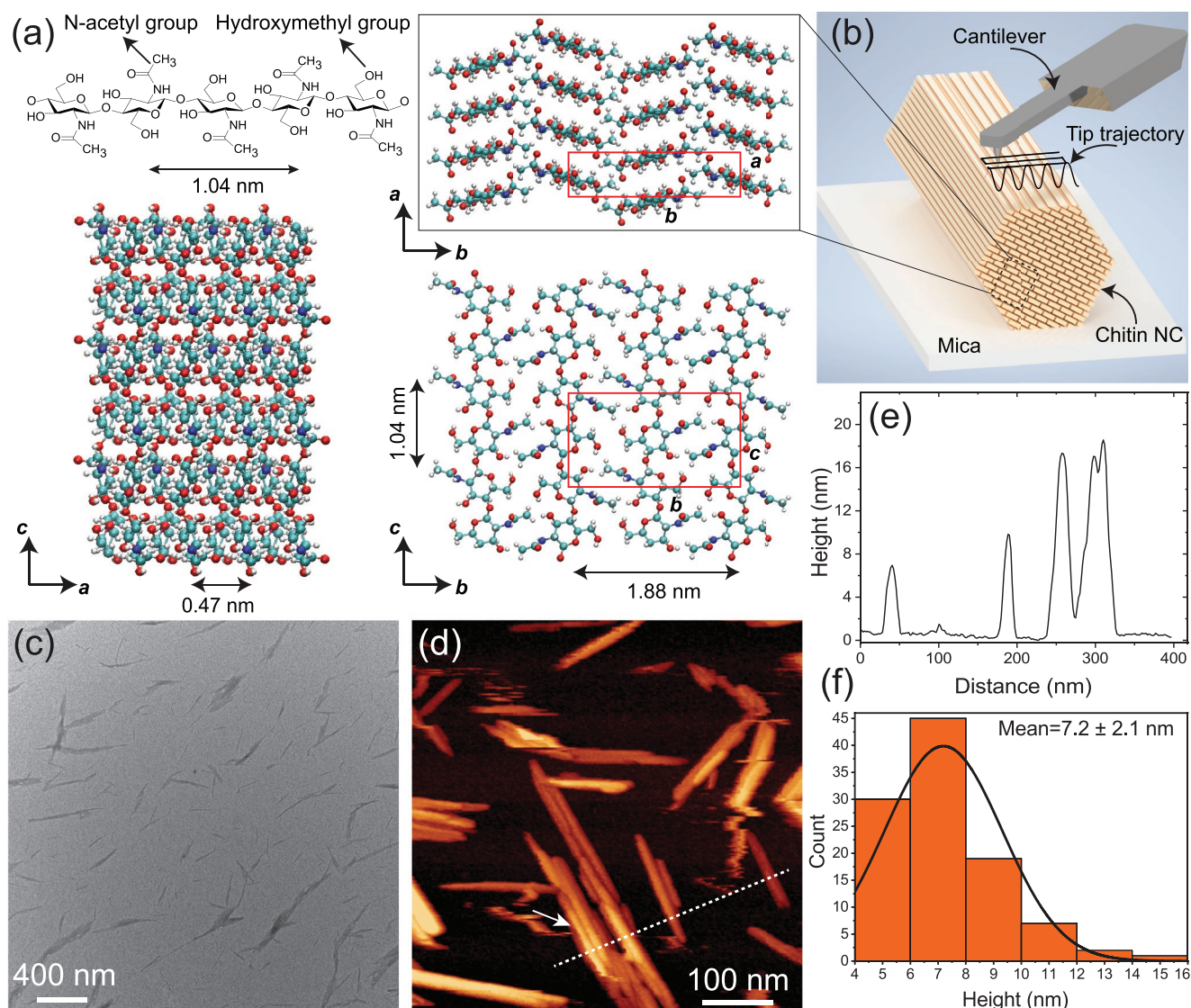


Figure 1. Overview of the chitin nanocrystal structure. a) The chemical structure of chitin (top left). The crystalline structure of α -chitin proposed by Sikorski et al.,^[22] viewed orthogonal to the ab -plane (top right), the ac -plane (bottom left), and the bc -plane (bottom right). The red rectangle indicates the unit cell. Carbon atoms are cyan, oxygen atoms are red, hydrogen atoms are white, and nitrogen atoms are blue. The crystal structure was obtained using the “chitin-builder” VMD plugin.[https://github.com/soft-matter-theory-at-icmab-csic/chitin_builder]. b) Schematic illustration showing the 3D-AFM on an individual chitin NC immobilized on a solid substrate. The tip scans both in Z and XY directions. The tip follows a sinusoidal trajectory as depicted in the schematic. c) A typical TEM micrograph of chitin nanocrystals derived from shrimp shells, prepared by acid hydrolysis. d) An AFM overview image of the chitin nanocrystals spread onto a freshly prepared mica substrate taken under water, revealing the presence of well-dispersed, quasi rod-shaped nanostructures. Some laterally aggregated particles also appear on the surface (white arrow). e) A representative line profile taken along the white dashed line shown in panel (d). The cross-section is averaged over ten lines parallel with the dashed line. f) Histogram showing the height distribution of individual chitin nanocrystals ($N = 110$) compiled from different AFM images. A mean height value of 7.2 ± 2.1 nm was obtained. We note that the large bundled nanocrystals were excluded from the height analysis.

depend on the chitin’s natural source. The most abundant and stable polymorph is α -chitin, where the interacting molecular chains are organized in an antiparallel arrangement in the unit cell as determined by the synchrotron X-ray diffraction studies.^[21–23] Antiparallel packing of α -chitin chains and the presence of the acetamino side groups lead to a high degree of hydrogen bonding that stabilizes the structure.^[24]

The nanoscale structural/morphological details and chemistry of chitin and other polysaccharide nanocrystals strongly influence their properties, such as crystallinity, liquid

crystal behavior, mechanical and rheological properties, and reinforcement efficiency in nanocomposites, and hence have a significant impact on their applications. However, there is limited knowledge on the molecular-scale details of the surface structure of chitin NCs, and their interface in an aqueous environment.^[19] In fact, a thorough molecular-scale characterization of the interactions at the chitin–water interface is critically important for chitin-based biomimetic material design, comprising of proteins/enzymes^[25] and understanding of some particular biological phenomena such as enzymatic

degradation activity of chitin^[26] and biomolecular assembly on chitin nanostructures.^[27] The realization of these biologically-oriented applications requires a precise characterization of the 3D structural organization of interfacial water molecules at the chitin surfaces. The structural and dynamical properties of interfacial water structuring were considered to be effective in mediating the interactions of chitin with other materials and biomolecules, and may play an essential role in determining the rates of enzymatic hydrolysis that takes place on chitin surfaces.^[28–31] Despite their importance, the molecular-level details of the chitin–water interfaces and the associated 3D hydration structures around the different surfaces of chitin NCs have never been experimentally reported. Here we provide the molecular-scale structural details of α -chitin nanocrystals (chitin NCs) isolated from shrimp shells in water by combining frequency modulation 3D atomic force microscopy (3D-AFM) experiments and molecular dynamics (MD) simulations. Highly-resolved AFM images provided the structural details of chitin chain arrangements on individual nanocrystal surfaces, revealing highly crystalline, well-ordered surfaces without many structural defects. We further visualize the 3D-interfacial hydration layers of structured water molecules on chitin NC surfaces with subnanometer resolution at the single-chain level. Our results showed that water molecules form stable, molecularly ordered hydration layer structures on the crystalline chitin surfaces. These structurally ordered layers of water molecules were found to encapsulate the surface of chitin NC inhomogeneously. The observed inhomogeneous water structuring reflects the amphiphilic surface character of chitin NCs with multiple crystalline planes with different chain arrangements and hydrogen-bonding ability. These findings were corroborated by the MD simulations, which predict similar water structuring that is determined by the specific arrangement of surface structural and chemical features. Our results could be crucial for exploring the chemical or enzymatic degradation at aqueous chitin interfaces and understanding the structure–property relationships occurring at chitin NC surfaces. This insight will be valuable for applications of chitin in a wide range of domains.

2. Results and Discussion

2.1. Structural Characterization of Chitin NCs

The morphology and size distribution of the chitin NCs prepared via hydrochloric acid hydrolysis were assessed by frequency modulation AFM (FM-AFM) and transmission electron microscopy (TEM) measurements. In Figure 1b, we show a schematic of 3D-AFM on a hexagonal-shaped chitin NC immobilized on a solid substrate. In the 3D-AFM method, the tip scans on top of the surface both in Z and XY directions. During linear XY scans, the tip follows a simultaneous sinusoidal trajectory in the Z direction as depicted in the schematic (see Section 5 for further details). A typical TEM micrograph of the α -chitin nanocrystals derived from shrimp shells is presented in Figure 1c. TEM images showed the presence of individual chitin fragments comprised of needle-shaped nanostructures with lengths of 100–600 nm and diameters of 10–20 nm. The

typical morphologies and sizes of the chitin NCs acquired by AFM in water are given in Figure 1d–f. The resulting AFM observations confirmed the presence of isolated and some laterally aggregated nanocrystals with homogeneous morphologies, similar to the TEM results. The formation of such chitin NC aggregates has been observed to occur due to the less-charged surface of the prepared NCs or incomplete fibrillation.^[32] The individual chitin NCs have typical lengths in the range from 100 to 300 nm and apparent widths in the range of 10 to 40 nm (a representative line profile across the several chitin NCs is shown in Figure 1e). Due to tip-convolution effects, the apparent diameters of the chitin NCs are relatively larger than their actual sizes. The AFM height measurements, which are not subjected to the tip-convolution effects, were used to determine the size of chitin NCs. The histogram analysis for the sizes of chitin NCs derived from different samples reveals height distribution in the range from 4 to 15.0 nm with a mean value of $7.2 \text{ nm} \pm 2.1$ (based on measurements of 110 individual chitin NCs with well-defined edges or boundaries)(Figure 1f), consistent with the average sizes reported for the chitin NCs from shrimps.^[33]

2.2. Molecular-Scale Image of Chitin–Water Interfaces

We further performed high-resolution FM-AFM observations to reveal the molecular details of the chitin chain arrangements at the surfaces of individual chitin NCs. We found that the surfaces of individual chitin NCs generally displayed extreme chain ordering over large domains covering almost the entire crystal surface (Figures 2 and 3; Figures S1–S8, Supporting Information). The surface exhibited a high degree of crystallinity, almost free of structural disorder or defects, indicating that the amorphous domains—mainly composed of proteins and minerals—are removed considerably by acid treatments while crystalline regions remain intact. An AFM topography image of α -chitin nanocrystals spread onto a freshly cleaved mica surface, acquired in water, is presented in Figure 2a, showing images of various individual chitin NC surfaces at a relatively lower resolution. Detailed molecular-scale structural characterization of various individual chitin NC surfaces was performed to determine the crystal lattice parameters. A representative AFM topography image presented in Figure 2b exemplifies such molecularly-resolved features of the chitin NC surface when imaged with the scan direction appropriately oriented. We found that interface structural features are best resolved when the chitin NC chain axis is oriented parallel to the probe fast scan direction or at an angle of 45° . A highly ordered molecular arrangement of crystal chains in the directions parallel and perpendicular to the fiber axis can be clearly discernible almost on the entire crystal surface without many major breaks (Figure 2b).

It is worth noting that at solid–liquid interfaces, the AFM tip is not only interacting with the surface features, but also with the ordered layer of water or solvent molecules formed above the sample surface. While the background forces experienced by the tip are dramatically reduced by water screening, leading to more localized force interactions and better imaging conditions, the origin of atomic/molecular scale contrasts observed

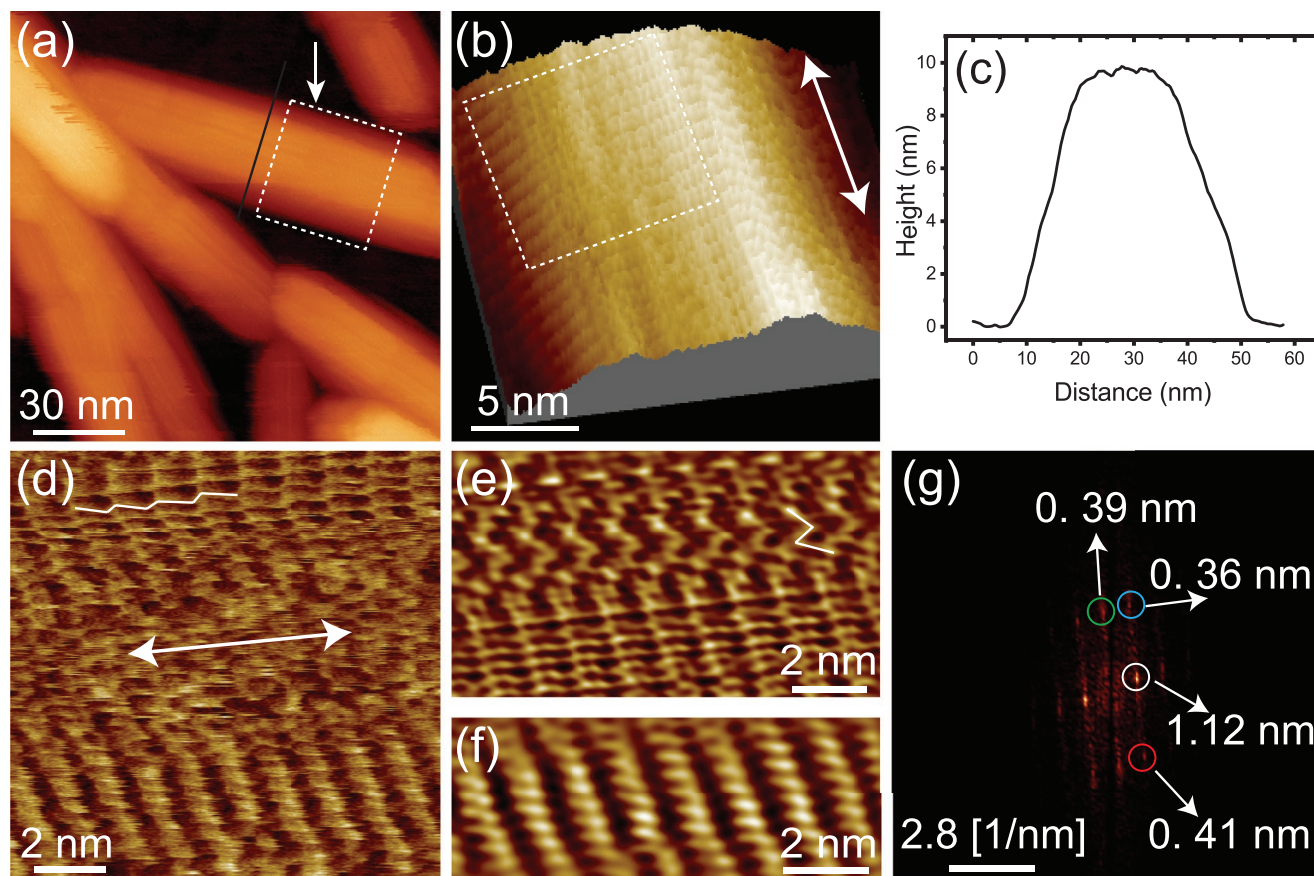


Figure 2. Molecular scale structure of chitin NC–water interfaces. a) An AFM topography image of α -chitin nanocrystals spread onto a freshly cleaved mica surface, acquired in water. b) A 3D rendering of an AFM topography image of the area in the white-dashed frame in (a), revealing the detailed surface structure of chitin NC at the molecular level. In (b), the scan direction was adjusted to resolve the surface features better. c) A representative line profile taken along the black line marked in (a). d) Enlarged AFM image of the region highlighted with a white dashed frame in (b). A zig-zag nature of the molecular arrangement of the chitin chains can be clearly resolved in the upper part of the image, while the bottom part of the image exhibits a stripe pattern with inner structures. e) The FFT-filtered reconstructed image obtained from the top part of the image data in (b). f) The FFT-filtered reconstructed image obtained from the bottom part of the image in (d). g) The 2D-FFT pattern taken from the image shown in (d). Five characteristic periodicities of 0.36, 0.39, 0.41, 0.55, and 1.12 nm are obtained from the FFT spectra. The double-headed arrows indicate the orientation of the chitin chains. The acquisition parameters were: $f_0 = 116.46$ kHz, $k = 26.3$ N m $^{-1}$, and $Q = 7.4$. Scan rate: 2.5 Hz (a); 5.5 Hz (b) and; 6.5 Hz (d).

in high-resolution AFM images in aqueous environments is a convolution of the tip-surface interactions and the interplay of hydration structures.^[34] Nevertheless, the molecular-scale AFM images obtained at chitin–water interfaces can provide insights into the crystallinity and lattice periodicity of the underlying chitin surface. Our AFM measurements and MD simulations validated that observed hydration structures are laterally commensurate to the underlying molecular-scale structures of the chitin NC surface (see Section 3).

A high-resolution molecularly-resolved AFM image of a small scan area marked by a white dashed-box in Figure 2b is shown in Figure 2d, which was acquired on a relatively flat part of the chitin NC (a cross-sectional profile taken along the black line in Figure 2a is shown in Figure 2c). The zigzag nature of the molecular arrangement of chitin chains can be seen in the upper part of the image, extending along the crystals' longitudinal axis (Figure 2d,e). The lower half of the image displays a rowlike pattern with detailed substructures (Figure 2d,f). Sequential AFM images taken above the surface area shown in Figure 2d confirm that the zigzag and rowlike chain features

are indeed reproducible (Figure S9, Supporting Information). There had been no tip changes or surface modifications. This supports the conclusion that the absence of a zigzag pattern in the lower half of the image might be due to the curved shape of the crystalline surface, where the AFM tip interacts differently with the relatively flat top part of the surface and the edges. A distinctly different type of molecular organization of the chitin chains was observed at the very top part of the AFM images in Figure 2b,e, where the zigzag arrangement of molecular features was found to be aligned perpendicular to the chitin chain axis. This could be explained because the surface functional groups might have different chain orientations and configurations. It might also be possible that the water molecules at the interface rearrange to maximize the interactions with chitin NC surfaces. The exposed surface hydroxyl and amide groups and some of the inter-chain hydrogen bonds that are lost at the surface form hydrogen bonds with the surrounding water molecules, leading to a different contrast pattern in high-resolution AFM images.^[35] The 2D-fast Fourier transform (FFT) pattern taken from the corresponding image data in Figure 2d

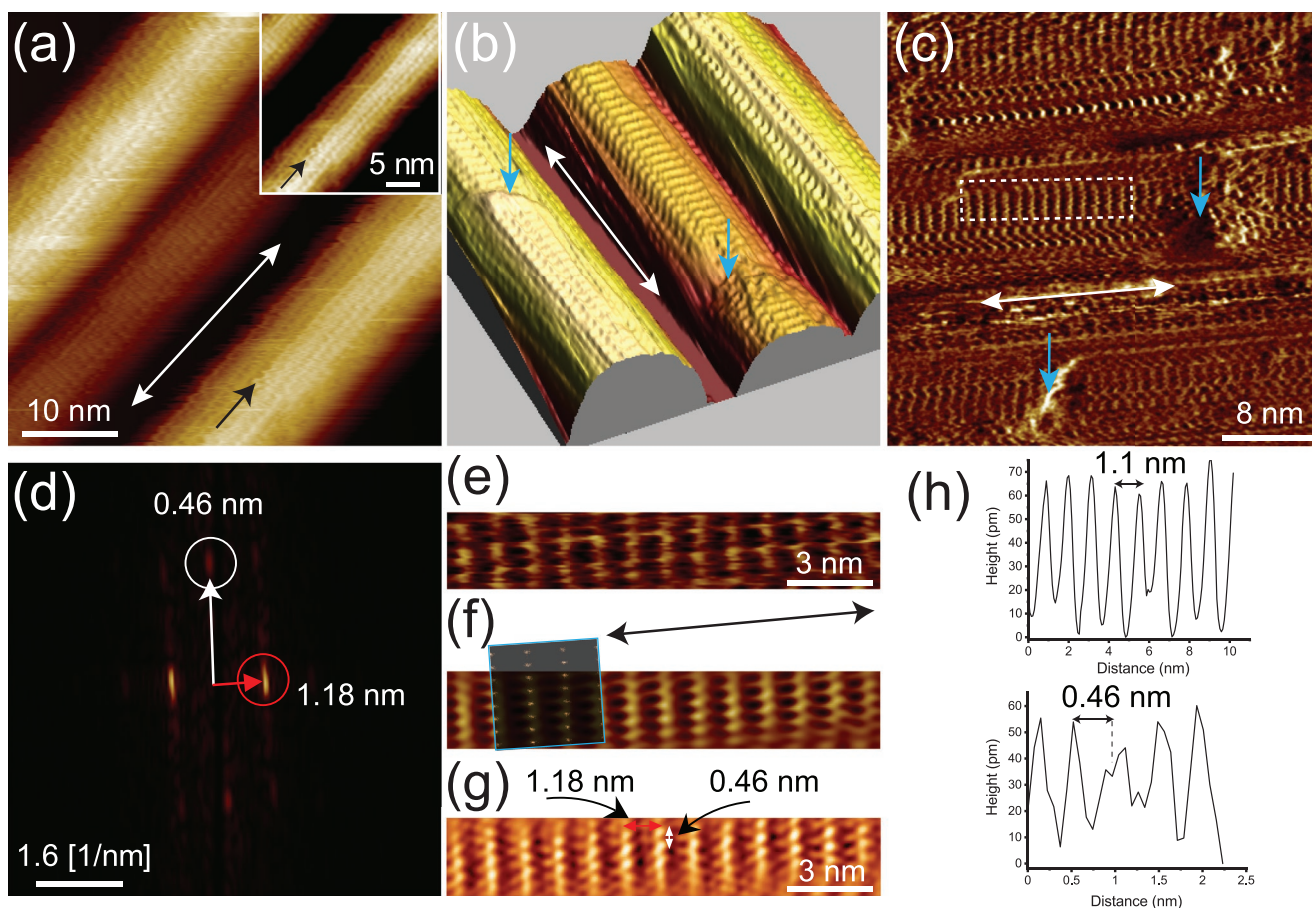


Figure 3. Ultrastructure of α -chitin nanocrystals. a) An AFM topography image ($45 \times 45 \text{ nm}^2$) of α -chitin nanocrystals adsorbed on mica surface taken in water. Inset shows magnified image of a part of the surface area, smoothed by a Gaussian blur. b) A 3D rendering of an AFM image ($40 \times 40 \text{ nm}^2$) of the same surface region shown in (a)–acquired with the fast scan direction parallel to the chain axis. Z-scale, 0–6 nm. c) Corresponding dissipation image data. Molecular-scale features at the interface of each chitin NC are clearly resolved. The blue arrows indicate the structural defects. d) The 2D-FFT pattern taken from the region marked with a white dashed frame in (c), confirming the characteristic unit cell parameters for the a and c axes, as determined in previous diffraction studies. e) Enlarged AFM topography image of the region highlighted with a white dashed frame in (c). f) The FFT-filtered reconstructed image obtained from (e), with an overlay representing the hydration structure near the (010) crystalline plane determined by the MD simulation. g) The corresponding FFT-filtered reconstructed dissipation image data. The spacing of bright protrusions along the chitin chain axis corresponds to that of the chitobiose repeating unit, while the spacing of bright features along the direction perpendicular to the chain axis corresponds to the a -axis of the unit cell. h) Representative line profiles taken along the direction parallel and perpendicular to the chitin chain axis. Chitin molecular chains run in the double-headed arrow direction. The acquisition parameters were: $f_0 = 140.02 \text{ kHz}$, $k = 38.8 \text{ N m}^{-1}$, and $Q = 7.9$. Scan rate: 6.5 Hz (a) and 6.0 Hz (b,c).

is indicated in Figure 2g. Multiple sets of characteristic peaks appear in the FFT spectra, showing the predominant periodicities of the surface features. The observed interval of 1.1 nm along the chain axis could be associated with chitobiose repeat distance (analogous to the cellobiose repeat) due to the two-fold screw symmetry of chitin chains.^[36] The other surface periodicities observed in the FFT spectra can be associated with the lateral molecular organization in the direction perpendicular to the chain axis. An inter-molecular spacing in the range of 0.39–0.42 nm was found, which is relatively smaller than the d spacing of the (010) crystalline plane. The measured periodicities in the lateral direction might be affected due to the curved structure of the surface (see further discussion below).

In the lateral direction perpendicular to the crystal axis, the one-phase molecular ordering exists only in a very local region extending over a short distance of a few unit-cell sizes,

making it difficult to determine the lattice parameters in the lateral direction. However, certain crystallographic planes, such as (010) planes of a hexagonal-shaped nanocrystal as proposed by Ogawa et al.,^[37] have a relatively large number of chains ordered with a relatively shorter periodicity. The molecular packing of chitin chains within the (010) plane is denser than within other crystalline facets. On such crystal planes, it is possible to determine the lattice parameters in the lateral direction as well. An example of such a situation is provided in Figure 3. In Figure 3a–c, we show high-resolution topography (in 2D and 3D perspective) and the corresponding dissipation images of the three-neighboring chitin NCs, respectively. The chitin NC chain axis in Figure 3b is oriented parallel to the probe fast scan direction, while that in Figure 3a is oriented at an angle of 45° . Molecular-resolution images enabled us to resolve the parallel individual molecular chains with substructural details

(see inset image in Figure 3a). In addition to the highly ordered crystalline domains, some minor disorder regions marked by blue arrows were also observed (Figure 3b,c). Although the chitin NCs were carefully washed, it might also be possible that these disordered domains are actually associated with some contaminants that prevent the high-resolution imaging of the crystal planes.

The 2D-FFT pattern taken from the area marked by a white-dashed box in Figure 3c is presented in Figure 3d, which can provide crystal parameters and surface periodicities for a specific crystalline plane. The corresponding enlarged AFM topography image of the region marked with a white dashed frame in Figure 3c is shown in Figure 3e. The FFT-filtered reconstructed images of the surface topography and the corresponding dissipation image data are also depicted in Figure 3f,g, respectively, displaying well-aligned molecular chains with detailed substructures in both lateral and perpendicular directions. An interval of 0.47 ± 0.04 nm between chains along the direction perpendicular to the chain axis and of 1.069 ± 0.036 nm along the chains was determined from the FFT spectra and line profile analyses taken from different samples (Figure S10, Supporting Information). The chitobiose repeat spacing was generally around 1.06 nm, although in some AFM images, it was higher (Figure 3d).

The molecular structure of α -chitin has been investigated previously by several researchers and revised several times.^[21,22] The most recent structural model was proposed by Sikorski et al.,^[22] which was based on the X-ray diffraction data from highly crystalline chitin obtained from crab shell (as depicted in Figure 1a). Previous high-resolution TEM analysis revealed the cross-sectional shape of an α -chitin microfibril from *Phaeocystis* as a hexagon.^[37] Based on the two-chain orthorhombic unit cell structure of α -chitin as proposed by Sikorski et al.,^[22] Ogawa et al.,^[37] constructed a molecular packing model for α -chitin NC. According to this molecular packing model, the observed periodicities of 0.47 and 1.06 nm can be assigned to the *a* and *c* axes of the two-chains orthorhombic unit cell,^[21] which has dimensions $a = 0.474$ nm, $b = 1.878$ nm, and $c = 1.032$ nm. Indeed, the crystallographic repeat distance of 0.47 nm closely matches the inter-planar lattice spacing along the *a*-axis of the (010)-planes as determined by the X-ray diffraction pattern from α -chitin.^[38] The presence of these two characteristic periodicities was also confirmed by the line profile analysis shown in Figure 3h, which are consistent with the imaging of the (010) facet of a hexagonal-shaped chitin NC surface. The observed relatively larger chain repeat distance along the main chain axis on the chitin NC surface could partially be attributed to the different minimum-energy of fiber repeats for chains in the interior and on the surface.^[39] The internal mechanical stress induced by the enforcement of hydrogen bonds between neighboring chains causes the chitin chains to compress (or stretch) to ensure identical repeat distances for all chains.

The molecular spacing along the *b*-axis was also determined by imaging the different crystalline planes (Figure S5, Supporting Information). As shown in Figure S5, Supporting Information, an interval of 2.1 nm was found between molecular chains, which is in good agreement with the value determined by our simulations for the (120) crystalline plane (Figure S5f, Supporting Information). These values appear to be fairly

consistent with the bulk lattice parameters of chitin NCs, suggesting that the surface structure of the crystal is not affected by the chemical and mechanical treatments during the preparation process. This also implies that water molecules at the interface do not cause many structural rearrangements of the chitin surface. However, they may refine the hydrogen-bonding network at the interface and improve the regularity of the lateral packing between chitin chains. This is reasonable because the water molecules enable the formation of hydrogen bonds similar to those in the interior bulk, giving rise to identical lattice parameters as the bulk crystal.^[35]

Various other molecular-scale, qualitatively different contrast patterns were also obtained on different chitin NCs; further examples from different samples are provided in Figures S1–S8, Supporting Information. The 3D morphological analysis through these crystals by AFM revealed that at a relatively lower resolution, the surface of chitin NCs exhibits a smooth rounded or flat morphology (Figure 1d; Figure S1a, Supporting Information), whereas, at the molecular scale, it displays a sheet-like stepped structure with step heights of 0.3–0.5 nm (Figures S1–S4, Supporting Information). The presence of distinctly different contrast patterns together with the observed stepped structures may imply that chitin NCs might have multiple surface planes exhibiting different molecular packing arrangements of chains and the intra- and inter-hydrogen bonding, corroborating the earlier finding of the multifaceted nature of α -chitin NC surface,^[37] as determined by the TEM cross-sectional measurements. However, we cannot rule out the possibility that the different orientations of the exposed *N*-acetyl glucosamine, hydroxymethyl, and OH groups on individual chitin chains could lead to distinct appearances of surfaces in high-resolution AFM images. The presence of water molecules may also change the distribution of H-bonding groups in chitin NCs. The competition between water and inter- and/or intra-molecular hydrogen bonds can lead to changes in the molecular arrangements on surfaces of crystalline chitin.^[40]

In some cases, the crystalline surface exhibits different domains. It does not show clear steps, but instead a relatively smooth transition between different domains occurs (Figure S6, Supporting Information). This might be due to the adaptation of different chain orientations and conformations in the crystal surfaces.

2.3. 3D-AFM Characterization of Hydration Structures at Chitin NCs–Water Interfaces

Next, we extend our discussion to the organization of water molecules at the chitin–water interface in more detail. We leveraged the high-resolution capabilities of 3D-AFM to characterize the interfacial water structuring. 3D-AFM has recently emerged as a powerful tool to provide unique structural information for various surfaces/interfaces and nanostructures with unprecedented detail, reaching molecular and atomic scales.^[41] It has been used to visualize the spatial distribution of 3D solvation structures formed on mica,^[42] calcite,^[43,44] ionic crystals,^[45] lipid headgroups,^[46] hydrophobic 2D materials (including, graphene, MoS₂, and WSe₂),^[47] condensed gas molecules on hydrophobic surface,^[48] heterogeneously charged surfaces,^[49] and purple

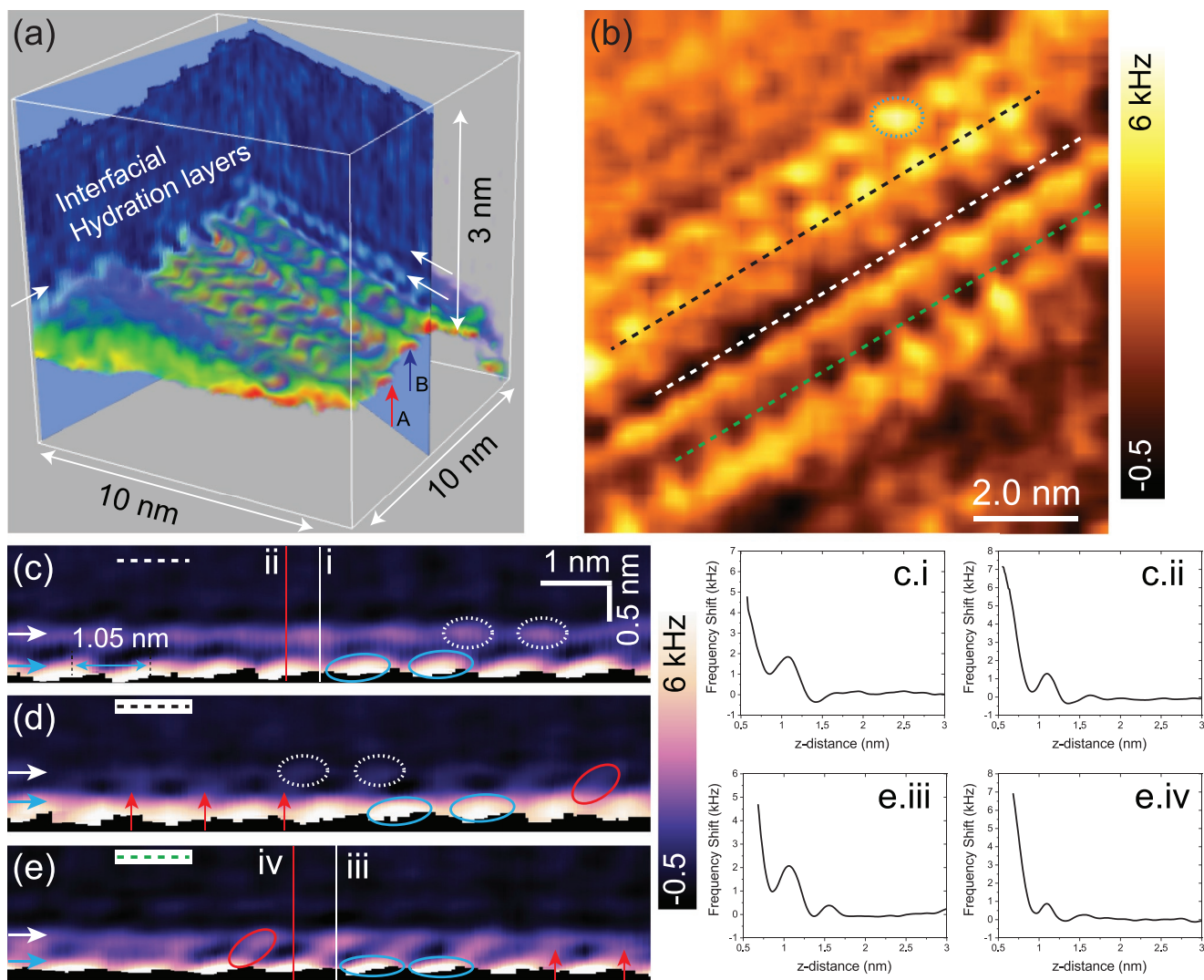


Figure 4. A representative 3D-AFM image of the chitin–water interface. a) 3D-AFM image of the chitin–water interface. The 3D map indicates the variations of the frequency shift of the oscillating cantilever as function of the xyz -coordinates. The molecular scale order can be seen in xz - and yz -planes highlighted by white arrows. b) Horizontal 2D- xy map of the chitin–water interface extracted from the 3D volume map at the vertical z -position marked by a blue arrow in (c). c–e) Vertical 2D cross-sectional maps of the chitin–water interface taken along the dashed lines marked in (b) that pass through the long-molecular chain direction, representing the presence of hydration layers. The red, white, and blue ovals indicate the ordered hydration features. c(i),c(ii)) Representative 1D frequency shift-distance curves taken along the white and red lines in (c), respectively. e(iii),e(iv)) 1D frequency shift-distance curves taken from 2D maps along the white and red lines in (e), respectively. The 2D cross-sections taken along the green, white, and black lines marked in (b) give a period of 1.05 nm between the hydration features, indicating the significant templating effect of the substrate. The force mapping area has a dimension of 10 nm \times 10 nm and is divided into grids of 256 \times 256 pixels. The frequency and amplitude of the z modulation signal during 3D-AFM force mapping were 195.3 Hz and 3 nm, respectively. The acquisition parameters were: $f_0 = 140.02$ kHz, $k = 38.8$ N m $^{-1}$, and $Q = 7.9$. Scan rate = 1.22 Hz. Scale bars are the same for (c–e).

membranes.^[50] All these measurements, however, were performed mainly on stable, atomically flat surfaces. The hydration measurements on curved surfaces with irregular shapes and heterogeneous chemistry are challenging^[51,52] because the particles are often displaced on the surface during scanning by a relatively stiff AFM cantilever, which is a prerequisite for the high-resolution imaging and characterization of the solvation structures.

After locating the individual chitin NCs on the mica substrate, we performed 3D-AFM force volume maps on a selected chitin NC surface with a typical resolution of 10 nm \times 10 nm \times 3 nm

(see Section 5 for further details). A representative 3D-AFM image of the chitin NC–water interface is provided in Figure 4a. The observed 3D map shows variations of the frequency shift (Δf) of the oscillating cantilever under the influence of interaction forces in 3D interfacial space. The overlaid vertical 2D xz and yz maps represent the structurally ordered water layers along the direction both perpendicular and parallel to the chitin molecular axis. Figure 4b shows the horizontal 2D- xy slice, reconstructed from the 3D- Δf map data at the vertical position marked with a blue arrow in Figure 4c, revealing the in-plane molecular organization of water molecules in the hydration

layer closer to the chitin surface. The images were flattened to visualize surface features better. Figure 4c–e shows three representative vertical 2D cross-sectional maps at different lateral positions taken along the white, black, and green dashed lines marked in (b), respectively. The resulting 2D cross-sectional maps reveal the interfacial water structures comprising of quasi-discrete layers of well-ordered molecular structures that lie horizontally to the chitin surface and extend to a height of about 1–1.2 nm from the underlying chitin NC substrate. These alternating bright/dark layers are indicative of hydration layers formed at the chitin–water interface, which were ascribed to the transition between the ordered layers of water molecules confined between the tip and surface.^[34,53] The arrangement of water molecules in the hydration layer was found to be laterally commensurate to the underlying chitin surface unit cell, as can be evidenced from the vertical 2D Δf maps (Figure 4c–e; Figures S7 and S8, Supporting Information) as well as from the conventional 2D-AFM images (Figures 3 and 4; Figures S4 and S5, Supporting Information). The periodicity of the molecular level features (marked with white dashed and blue ovals) along the chain axis closely matches the fiber repeat distance of 1.05 nm.

It can be seen from the vertical 2D maps that the hydration layers (marked with white arrows) are discretely interconnected to the below hydration layers through the inner layer water molecules (indicated by red arrows), occupying the space between the prominent hydration features closer to the chitin surface (blue ovals). However, the water molecules in the inner hydration layers are not directly located at the center between these hydration features, but are slightly shifted from the center and tilted toward the neighboring one (red ellipse in Figure 4e). The single 1D Δf -distance curves taken from different positions on the 2D- xz maps showed a strong repulsive force when the tip is positioned between the hydration features marked with blue ovals (Figure 4c(i),e(iii)), indicating the presence of confined water molecules. The closest approach of the tip toward the hydrating water molecules located at these positions does not cause any changes in their positions or structures, suggesting the presence of strong hydrogen bonding between water molecules and the surface OH groups. Our hydrogen bond analysis indeed confirmed the presence of a large number of hydrogen bonds between water molecules and chitin hydroxyl groups (see Figure 6).

On the other hand, we observe the formation of a hydration structure, with characteristic empty gaps (dark contrast) located either directly on top of the hydration features closer to the chitin surface (marked with blue ovals in Figure 4d) or between the inner layer water molecules (marked with red arrows). This type of hydration pattern has been reported in previous MD simulations for analogous aqueous cellulose interfaces,^[35,54] representing the local absence of water molecules. Due to the hydrophobic character of pyranose rings, the water molecules near these regions are expelled from the interface, leading to a water-depleted region above these sites.

The vertical 2D slices through the z -plane in the perpendicular direction to the chain axis differ considerably from that in the parallel direction to the chain axis. The averaged vertical 2D maps in the perpendicular direction reveal undulating hydration profiles with relatively higher molecular corrugations and

wider grooves (Figure S7d, Supporting Information), in contrast to a horizontal flat density profile along the chain axis (Figure 4; Figures S7c and S8d,e, Supporting Information). The 3D maps of chitin–water interfaces taken from different samples showed that these interfacial structured water layers occur across the entire xy -plane of chitin NC surfaces. However, they are not uniform but located in certain regions with increased density and consist of several different molecular patterns (Figures S7 and S8, Supporting Information).

We performed MD simulations to provide a molecular-level understanding of the observed hydration structures around the chitin NC surfaces. A hexagonal-shaped multifaceted crystalline structure for α -chitin NC was constructed to capture the details of the molecular arrangement of the interfacial water molecules (Figure 5a; Figure S11, Supporting Information), see further information Section 5 (Computational Details). As mentioned earlier, the hexagonal-shaped molecular packing structure has been previously observed by TEM cross-section measurements for α -chitin NCs.^[37] From the MD simulation trajectories, we calculated the number of hydrogen bonds (HBs) formed between water molecules at the interface and the possible sites at the crystalline α -chitin surface to explain the observed hydration patterns along the chitin chain axis (Figure 4c–e). The largest number of hydrogen bonds was detected between water molecules and chitin hydroxyl groups (Figure 6a). The second most common type of hydrogen bond is formed between water molecules and oxygen atoms in the *N*-acetyl glucosamine side groups (labeled as O14 in Figure 6b). The interaction with the OH groups is the most prominent, with water both donating its hydrogen to the hydroxyl oxygen (labeled as O11) as well as accepting the hydrogen from the OH group. This is understandable because this OH group is one of the main functional groups that form intermolecular HBs between chitin chains, and being depleted of those interactions at the surface, it is prone to form further HBs with the surrounding water molecules. Also noticeable are the HBs formed between the *N*-acetyl glucosamine side group with water oxygen, although those are in much less quantity than the previous interactions discussed. Other combinations, such as water interacting with the nitrogen atom acting as acceptor as well as oxygens labeled as O12, O13 are much less pronounced.

The high tendency of water molecules to form HBs with surface OH groups and the confinement of the water molecules around the hydrophobic CH-exposed regions lead to the localization of high-density regions around the OH group sites, which is consistent with the above interpretation of hydration structures shown in Figure 4c–e. The regions marked with blue and red ovals in Figure 4c–e correspond to the areas where water molecules are stabilized by a hydrogen bond with either the hydrogen or oxygen atom of the hydroxy groups in the chitin chain, and the regions with darker contrast (empty gap) in between these regions correspond to the regions where water molecules generally make no hydrogen bonds with the chitin surface. A comparison of experimental and simulated hydration patterns along the chitin chain axis is demonstrated in Figure S12, Supporting Information, indicating a reasonably good agreement.

The simulated density contours of water molecules around all exposed crystalline planes are demonstrated in Figure 5b, indicating that the water molecules are highly structured by

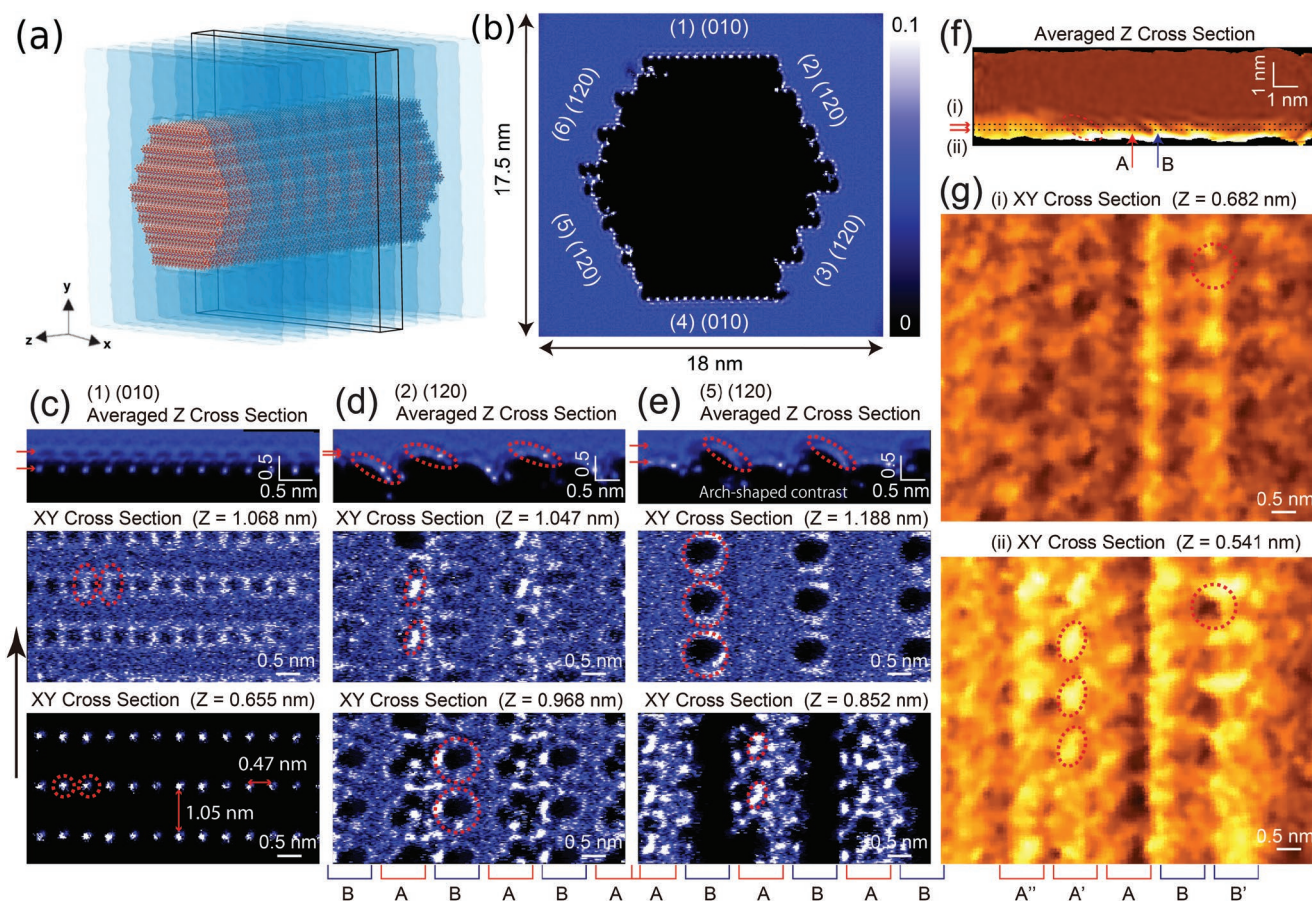


Figure 5. Comparison of simulated water density distribution with experimentally observed hydration structures. a) Model structure for chitin NC employed by the MD simulation, exposing different crystallographic planes. b) Calculated 3D water oxygen density map around the six exposed crystalline planes. c–e) Averaged 2D density profiles of water oxygen atoms in the vertical zx -plane at the interfaces labeled with numbers 1, 2, and 5, respectively (top). Bottom and middle; horizontal 2D- xy maps extracted from the 3D density map, showing the in-plane interfacial water density distribution for different vertical z -positions. The red arrows indicate the vertical positions where the 2D- xy maps were extracted from the 3D map. The high water density regions are indicated by red ellipses. f) Averaged vertical 2D Δf profile taken along the direction perpendicular to the chitin chain axis. The arrows marked with letters A and B indicate the same positions as Figure 4a. g) Experimentally obtained 2D- xy maps of chitin–water interfaces extracted from the 3D- Δf map shown in Figure 4a for two vertical z -positions marked with red arrows in (f). The letters point to identical hydration features. The black arrow on the left indicates the chitin molecular axis.

the chitin surface. The resulting MD simulations furthermore revealed molecular-level differences in the structure of water layering at these different crystalline interfaces with distinct chain packing and hydrogen bonding capability, reflecting the heterogeneous character of the interactions at the chitin–water interfaces (Figure 5b). A detailed comparison of simulated 2D horizontal and vertical water oxygen density maps above the six crystalline planes is provided in Figures S13–S15, Supporting Information. Similar to the experimental results, the simulated interfacial water structures at these six interfaces represent the symmetry of crystalline chitin, indicating a strong templating effect that the underlying surface has on the resulting hydration structures.

The vertical 2D- xz and horizontal 2D- xy water density maps at the (010) surface facets labeled with numbers 1 and 4 show identical hydration patterns as expected, with both exhibiting the regularly arranged hydration features with a periodicity of 0.47 nm in the direction perpendicular to the chain axis and of 1.05 nm parallel to the chitin molecular axis (Figure 5c;

Figure S13, Supporting Information). The simulated xy contour map above the (010) crystalline plane—extracted at a distance closer to the chitin surface (lower panel in Figure 5c)—shows a striking resemblance with the hydration structures observed in experiments (Figure 3f). The hydration structure determined above the (010) crystalline plane (Figure 5c) is overlaid on Figure 3f for comparison.

The water–oxygen density profiles predicted for the (120) surface facets, on the other hand, displayed some quantitatively different hydration patterns (Figure 5d,e). As evidenced from the averaged 2D water oxygen density profiles taken through the z -plane in x or y direction, the (120) surface planes labeled with the numbers 3 and 6 exhibited higher surface roughness with relatively deeper and wider grooves than the crystalline planes labeled with the numbers 2 and 5 (the groove depth being approximately twice as large, Figure S13b, Supporting Information). Given the relatively smaller roughness of chitin molecular structures, the hydration structures determined at the 3 and 6 interfaces do not agree with the results obtained

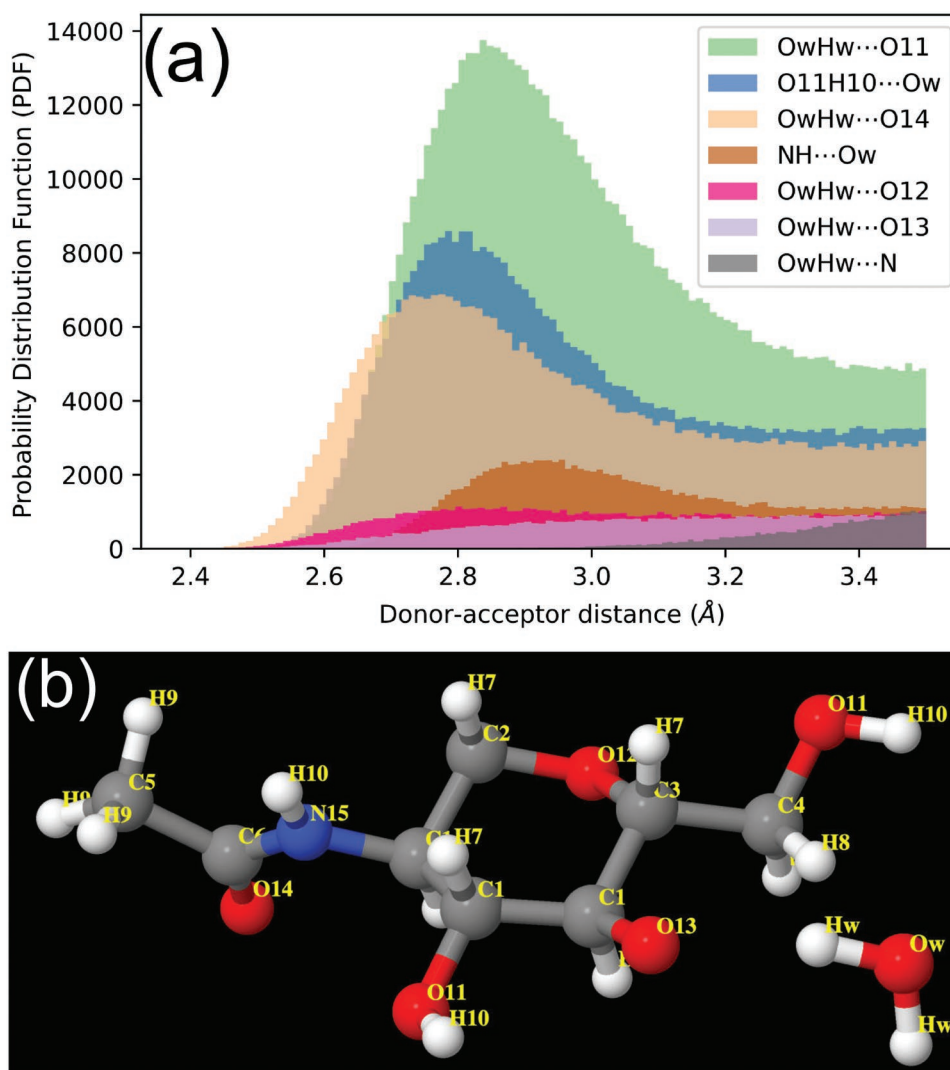


Figure 6. a) Hydrogen bond analysis between the possible chitin sites and water molecules. b) Atomic structures of chitin and water with the respective labels used in the hydrogen bond analysis. Chitin and water molecules are displayed in a ball-and-stick model.

from our experiments. This discrepancy might be due to difficulties in probing such highly inclined and corrugated surface planes by AFM.

To further compare our simulations with the experiment, we examined in detail the vertical and lateral organization of water molecules at the 2 and 5 crystalline planes for different vertical z -positions. In Figure 5d,e, we showed the averaged vertical 2D- xz density maps of water oxygen atoms at the crystalline planes of 2 and 5, respectively, which were taken along the direction perpendicular to the chain axis. The MD simulations revealed the formation of arc-shaped hydration patterns (some of them marked with red dashed ellipses), which are in good agreement with the experimentally obtained vertical 2D- Δf profiles taken along the direction perpendicular to the chain axis (Figure 5f; Figure S7d, Supporting Information). The simulated 2D vertical water density profiles closely follow the contours of the surface molecular corrugations (Figure S14, Supporting Information), resulting in an undulating appearance, similar to the AFM experiments. However, in AFM

experiments, the 2D- xy maps exhibit a significant degree of variability in the periodicity of the surface features in the lateral direction, likely resulting both from the influence of the tip structure and tip-induced mobility.^[55,56] As detailed in Figure S14, Supporting Information, the water molecules approach closer to the crystal surface either above the surface sites between the chitin chains or through the surface grooves and form hydrogen bonds with the exposed surface OH groups in the chitin chains.

To gain further insight into the water structuring, we extracted the 2D density maps of in-plane interfacial water distributions at these interfaces, as shown in the middle and lower panels of Figure 5d,e. The red arrows (shown in Figure 5d,e) indicate the vertical positions where the 2D- xy density maps were extracted from the 3D density map. The 2D water oxygen density maps determined by MD simulations show regularly ordered dark, blue, and white features, indicative of low, moderate, and high water density. These regularly arranged features (red ellipses and circles) in density maps are observed

to be aligned parallel to the main chain axis (black arrow), agreeing well with the corresponding experimentally observed 2D xy hydration patterns, where the molecular-level features are running parallel to the main chain axis (Figures 4 and 5g; Figure S8c, Supporting Information). Evaluation of the lateral xy slices is observed when moving from the vertical distance of $z = 1.047$ to $z = 0.968$ nm (Figure 5d), where the high water density regions along the chain axis in 2D- xy maps are shifted to the right. This local arrangement of water density is consistent with the experimentally determined hydration patterns shown in Figure 5g, and it reflects the surface anisotropy.

3. Discussion

Chitin nanocrystals offer great potential as fibrous reinforcement in nanocomposite materials. It has been demonstrated that the presence of polysaccharide-based nanocrystals in a polymer matrix greatly increased the stiffness and tenacity.^[57] The improved mechanical properties were mainly attributed to the combined effect of increased crystallinity of polymer microstructure and direct reinforcement by the polysaccharide nanocrystals. However, the surface crystallinity of individual chitin NCs in an aqueous environment has not been elucidated in real-time by microscopic techniques. The nanomechanical properties of chitin nanocrystals are mainly determined by their crystallinity,^[58] which is related to the atomic/molecular arrangement and molecular chains' orientation on the crystal surface. High-crystallinity of the chitin NCs in an aqueous environment is a prerequisite to use them as nano-fillers in nanocomposites with better mechanical properties, as lower crystallinity of surfaces in a composite nanostructure decreases the mechanical strength of the resulting nanomaterials.^[59] The nanostructures with large aspect ratios and high crystallinity showed high mechanical strength and thermal stability.^[60] Consequently, they might be expected to have higher physico-mechanical characteristics,^[61] such as higher elastic moduli. The crystallinity of chitin NCs also determines their accessibility to chemical reagents, and the high crystallinity of chitin surfaces would make them more resistant to chemical and enzymatic hydrolysis. These unique characteristics make them ideal candidates as nano-reinforcing fillers for composite nanomaterials.

We characterize the 3D local hydration structures around the different surfaces of chitin NCs with subnanometer resolution at the single-chain level. Our results showed an inhomogeneous water structuring that covers the entire chitin NC surface. 2D vertical and horizontal Δf maps in AFM experiments and the corresponding 2D water density profiles in MD simulations revealed that the interfacial water structures are strongly affected by the topographic contours and exposed chemical moieties of different crystalline interfaces. This inhomogeneous water structuring reflects the amphiphilic character of crystalline α -chitin, including both hydrogen bonding and hydrophobic interactions. The interactions of solvent molecules with chitin NCs at the interfaces govern the interactions among the chitin NCs and influence the interfacial shear properties,^[62] which could, in turn, affect the percolation properties of chitin NCs within the composites and thus play a crucial role in the reinforcement efficiency and the performance of resulting nanocomposites.^[63]

All biological relevant processes involving chitin occur at the chitin–water interface. The details of solvent structuring at the interface region significantly affect the rate of diffusion of external molecules toward surfaces; thus, the hydration structure could play an important role, for instance, in controlling the nature and rates of chemical reactions, such as enzymatic hydrolysis of chitin.^[54] A solvent-mediated interaction has been suggested for peptide–Au and titania in water,^[64] where the adsorbate molecules initially recognize the hydration layers at the interface, not directly the surface itself. An inhomogeneous presence of hydration layers at the chitin–water interface suggests that certain surface facets might have different electronic properties and exhibit different properties against, for instance, molecular adsorption, diffusion, and chemical/hydrolysis reactions.^[54] The differences in the electrostatic properties of different crystalline facets were confirmed by MD simulations, where the crystalline planes labeled with numbers 1, 2, and 3 exhibited a distinct charge density distribution (Figure S16, Supporting Information). This difference influences the interactions between chitin surface and external bio-molecules, such as proteins and peptides^[65] and may confer selective adsorption of external molecules on certain surface facets.

4. Conclusion

The characterization of chitin NC surfaces at the atomic/molecular resolution is a remarkable result that will substantially advance the understanding of chitin nanocrystals' surface chemistry and provide a more in-depth insight into the structure–reactivity relationships that take place on chitin NC surfaces. This could also pave the way for assessing the chemical and enzymatic activities on chitin NCs, offering understanding of the mechanisms of chitin degradation, which is crucial for biomass conversion.^[66] Furthermore, the detailed characterization of the 3D local hydration structures with molecular resolution at different chitin–water interfaces would contribute to a better understanding of biomolecular binding to chitin NCs, such as chitinases and chitin-binding proteins, which are essential for the crystalline chitin hydrolysis.^[31] Our findings might provide a basis for designing an effective strategy for the molecular and chemical processes to modify or decompose chitin NCs.

5. Experimental Section

Materials: Chitin from shrimp shells (practical grade, powder; Sigma-Aldrich), hydrochloric acid (37 wt% in water; Sigma-Aldrich), and hydrogen peroxide solution (30 wt% in water; Sigma-Aldrich) were used without further purification. Centrifugation was performed on an Eppendorf Centrifuge 5804 R equipped with Falcon 50 mL polypropylene conical centrifuge tubes. A Durasonix Ultrasonic Cleaner DR-MH30 (ultrasonic power of 120 W, frequency of 40 kHz) was used for sonication treatments. Dialysis tubing cellulose membrane (average flat width 33 mm, typical molecular weight cut-off = 14 000; Sigma-Aldrich) was used in the dialysis experiments.

Chitin Nanocrystal Preparation: The chitin nanocrystals were prepared according to a literature procedure.^[67] To a 500-mL two-necked round-bottom flask equipped with a magnetic stir bar and a reflux condenser were added 10.0 g of chitin powder and an aqueous solution of hydrochloric acid (200 mL, 4.0 mol L⁻¹). The above mixture was refluxed at a temperature of

378 K and a stirring speed of 1200 RPM for 18 h. Afterward, while keeping the temperature and stirring speed unchanged, an aqueous solution of hydrogen peroxide (30 wt%, 10.0 mL) was slowly added to the flask over a period of about 5 min, then the mixture was stirred at 1200 rpm and 378 K for another 30 min, during which time the dark brown byproducts were bleached. At the end of the reaction, the system was cooled down to room temperature. The chitin nanocrystals were separated as a solid product by centrifugation (2000 rpm, 20 °C, 30 min), then redispersed in about 100 mL of deionized water by sonication, and dialyzed against deionized water (1.5 L × 10 times, 24 h each time) to remove residual electrolytes until the external solution reached a neutral pH and a homogeneous colloidal dispersion was formed inside the dialysis tube. In a typical experiment, the finally obtained dispersion of chitin nanocrystals had a pH of about 6–7 and a concentration of 3.35 wt%. The prepared chitin NC suspensions were stored at 4°C until use.

TEM Characterization of Chitin Nanocrystal: The morphology of chitin nanocrystals was observed by TEM. TEM observations were conducted on a Hitachi H7600 electron microscope at an accelerating voltage of 80 kV. Samples for TEM imaging were prepared by drop-casting an aqueous dispersion of chitin nanocrystals (about 0.005 wt%, sonicated for 30 min before using) onto carbon-coated copper grids.

Preparation of Chitin Suspension for AFM Observations: An aqueous suspension of chitin nanocrystals (3.35 wt%) was first diluted into a concentration of 0.0133 wt% in Milli-Q water. The suspension was then sonicated using an ultrasonic homogenizer (MITSUI, 3 mm diameter tip, and a maximum power of 500 W). The aqueous suspensions of chitin samples were placed in an ice bath to prevent the excessive heating generated during the sonication process and sonicated four times for 3 min. The chitin NCs suspensions used in AFM studies were prepared by placing a drop of the dilute specimen (100 µL) onto a freshly cleaved mica substrate. After incubation for 25 min, the mica substrate was rinsed with 100 µL of Milli-Q water several times to lower the concentration of chitin NCs further and remove unbound chitin NCs entities. A brief sonication post-process was performed before placing chitin NC suspension on a freshly prepared mica substrate to prevent the formation of chitin NC aggregates. Since the prepared chitin NCs have positively charged surfaces (at pH of 6-7), as demonstrated by Zeta potential measurements (not shown), the chitin NCs were found to bind tightly enough on the negatively charged muscovite mica substrate by electrostatic interactions to be appropriately observed by AFM in a liquid environment. Milli-Q deionized water with a resistivity of 18.2 MΩ.cm was used throughout the experiments.

FM-AFM Setup: The surface and interface structural characterization of chitin NCs were realized with a homemade frequency modulation AFM (FM-AFM) system operating in liquid environments equipped with an ultra-low noise cantilever deflection sensor.^[68] The oscillation of the AFM cantilever was driven by photothermal excitation with an infrared laser beam with a wavelength of 785 nm. The homemade AFM scanning was controlled by a commercial AFM controller (ARC2, Asylum Research), and the amplitude of cantilever oscillation was kept constant using a commercially available controller (OC4, SPECS). The AFM was operated in constant frequency shift (Δf) mode, where the tip-sample distance was adjusted such that Δf is kept constant. The AFM images were acquired with 160AC-NG cantilevers purchased from OPUS with a nominal spring constant of 26 N m⁻¹ and a nominal tip radius <8 nm. The individual spring constant of each cantilever using the standard thermal tune method was experimentally determined.^[69] The scan rates and scan angle were adjusted to obtain a better resolution of the surface features. AFM image rendering and data processing were performed by using the WSxM and Gwyddion image analysis software. No filter was applied during the AFM scanning process. The cantilevers, in some cases, were coated with Si (15 nm) by a dc sputter coater (KST-CSPS-KFI) to enhance the tip-apex stability and remove the tip-apex contaminants. The drift velocities along the *x* and *y* directions are 0.0044 and 0.0035 nm s⁻¹, respectively.

3D-AFM Measurements: The 3D force or Δf maps of chitin–water interfaces were realized using the 3D-AFM force mapping method developed by Fukuma et al.^[41] In the 3D-AFM technique, the tip is scanned vertically and laterally to probe the interaction forces

acting between the tip and surface in the 3D interfacial space. A fast-sinusoidal signal was applied to change the tip's *z*-position during image acquisition and force mapping. During tip linear *XY* scans, Δf is recorded for each tip position while the averaged tip-sample distance is regulated so that the average value of the Δf set-point is kept constant. A 3D Δf map with high-spatial-resolution can be obtained by recording in real time the force field acting on the tip for each tip position in the three spatial coordinates.

The main difference between the conventional 2D/3D-AFM and the 3D-AFM method used in this study was the use of *Z* modulation signal during 2D *XY* scans. The other 3D-AFM methods had no tip-sample regulation during the tip *XY* scans and were extremely slow.^[70] The fast acquisition speed of 3D-AFM made it suitable for imaging in liquid environments, where non-linear drift was always present and was extremely difficult to prevent.^[71]

Visualization of the oscillatory Δf -distance profiles—which indicate the structured interfacial water layers—required cantilever oscillation amplitudes smaller than the size of a water molecule. The cantilevers were driven photothermally at their resonance frequency with oscillation amplitudes set in the range of 0.1–0.25 nm to resolve the distribution of local hydration layers. The frequency and amplitude range of the *z* modulation signal during the 3D-AFM force mapping were: 195.3 Hz and 3–4 nm, respectively. To map the interfacial hydration structures, a large-area scan of the surface was first performed to locate the individual chitin NC that will be used to investigate hydration shell structures. Localized surface imaging in smaller scan areas to map the surface topography using the standard 2D FM-AFM imaging mode was then performed. Then it was switched to the 3D-AFM method to map the local 3D-hydration structure. On a selected surface area, a 3D- Δf map covering an area of 5–10 × 5–10 nm square—divided into grids of 128 × 128 pixels—was acquired by recording in real time the Δf with respect to the tip positions in 3D interfacial space on the chitin NC surface. The *z* data of the 3D map included 256 pixels. Note that for a stable force mapping process, in some cases, the dissipation channel was used as a feedback signal to adjust tip-sample separations. It should also be noted that the observed peak maxima in the Δf curves were interpreted as maxima in the water density distribution, based on the solvent tip approximation model.^[34] The validity of this model had been demonstrated on different solid–liquid interfaces^[34,49,55,56,72] (see Section S3, Supporting Information).

3D-AFM Data Processing: A homemade data analysis software based on a Labview program was used to process the large-size 3D force mapping data and extract the 2D section maps at different vertical and lateral positions. The following processes were performed to acquire the 3D force maps. The baseline correction was initially performed for a region far from the surface, where the force values at far tip-sample distances were aligned at zero force value. The slope of the surface was then corrected by subtracting the average height from each line scan. Then, the height correction was performed. The resolution of 3D- Δf data was increased by linear interpolation. Finally, the 3D Δf data were filtered using a 3 × 3 averaging filter. The details of 3D-analysis software could be found in ref. [53].

Computational Details: The chitin structure and topology were obtained by modifying the “chitin-builder” VMD plugin (<https://github.com/soft-matter-theory-at-icmab-csic/chitin-builder>), to create a hexagonal-shaped structure instead of rectangular ones. The generated structure consisted of a hexagonal–chitin crystal unit cell repeated three times along the *z*-direction. The crystal was solvated using Packmol^[73] in a box of size 26.65 nm × 26.42 nm × 3.15 nm, periodically repeating in all directions to simulate an infinite NC. The system consisted of 152 952 atoms in total (47 952 for chitin and 105 000 for water). The MD simulations were carried out using the LAMMPS package,^[74] and input files for LAMMPS were prepared with Moltemplate.^[75] The CHARMM36 force field with the TIP3P water model was employed to describe the chitin inter-atomic interactions and capture the chitin–water interactions. It has been shown that CHARMM36 described this system well.^[76] The system was equilibrated for 4 ns, using an integration time step of 1 fs. The production run was carried out in the NVT ensemble for 10 ns, using a Nosé–Hoover thermostat with *T* = 300 K and a damping

parameter $\tau = 0.1$ ps. Lennard–Jones interactions were computed with a 9 Å cutoff, while for the electrostatic interactions, the Particle-Particle-Particle-Mesh (PPPM) solver^[7] was employed using a 12 Å cutoff for real-space electrostatics and an accuracy of 10^{-6} . Hydrogen bond analyses were done with the MDAnalysis software.^[78,79] The criteria utilized for identifying hydrogen bonds were a maximum distance of 0.35 nm between water–oxygen and chitin–oxygen/nitrogen and a donor-hydrogen-acceptor angle of 100° . Finally, oxygen water densities were extracted using MDAnalysis, using a 0.1 Å grid spacing and a total of 1000 frames, each sampled every 10 ps during the production run.

Supporting Information

Supporting Information is available from the Wiley Online Library or from the author.

Acknowledgements

The authors gratefully acknowledge financial support by Grants-in-Aid for Scientific Research (Nos. 20H00345 and 20K05321) from the Ministry of Education, Culture, Sports, Science, and Technology of Japan (MEXT). This work was also partly funded by JSTMirai Program (No. 18077272). The authors thank the World Premier International Research Center Initiative (WPI); MEXT, Japan; and the Kanazawa University Fund (Strategic Research Promotion Program, Core-to-Core Program). The authors also acknowledge financial support from the Sumitomo Foundation (No. 190382), the Natural Sciences and Engineering Research Council (NSERC Canada) (Discovery Grant F16-05032). This work was a part of the Academy of Finland's Flagship Programme under Projects No. 318890 and 318891 (Competence Center for Materials Bioeconomy, FinnCERES) and also Project No. 314862. Computing resources from the Aalto Science-IT project and CSC, Helsinki are gratefully acknowledged. Figure 2 was updated on September 20th 2022 after initial online publication.

Conflict of Interest

The authors declare no conflict of interest.

Author Contributions

A.Y., T.F., M.J.M., and A.S.F. conceptualized the study and designed the experiments and simulations. A.Y. performed the 3D-AFM measurements, and analyzed the data. P.W. and M.J.M. prepared the chitin nanocrystals. K.M. helped with the data analysis. F.P. and Y.M.J. performed the MD simulations. A.S.F. supervised the MD simulations. A.Y. wrote the manuscript with input from all authors.

Data Availability Statement

The data that support the findings of this study are available in the supplementary material of this article.

Keywords

α -chitin, atomic force microscopy, chitin nanocrystals, chitin–water interactions, hydration layers, molecular dynamics simulations, polysaccharides

Received: March 14, 2022
Revised: May 4, 2022
Published online: June 9, 2022

- [1] Y. Zhu, C. Romain, C. K. Williams, *Nature* **2016**, *540*, 354.
- [2] F. J. Martin-Martinez, K. Jin, D. López Barreiro, M. J. Buehler, *ACS Nano* **2018**, *12*, 7425.
- [3] N. Lin, J. Huang, A. Dufresne, *Nanoscale* **2012**, *4*, 3274.
- [4] M. Giese, L. K. Blusch, M. K. Khan, M. J. MacLachlan, *Angew. Chem., Int. Ed.* **2015**, *54*, 2888.
- [5] J. A. Kelly, M. Giese, K. E. Shopsowitz, W. Y. Hamad, M. J. MacLachlan, *Acc. Chem. Res.* **2014**, *47*, 1088.
- [6] Y. Wang, L. Chen, *ACS Appl. Mater. Interfaces* **2014**, *6*, 1709.
- [7] R. Sinko, X. Qin, S. Keten, *MRS Bull.* **2015**, *40*, 340.
- [8] K.-Y. Lee, T. Tammelin, K. Schulfter, H. Kiiskinen, J. Samela, A. Bismarck, *ACS Appl. Mater. Interfaces* **2012**, *4*, 4078.
- [9] H. Dong, K. E. Strawhecker, J. F. Snyder, J. A. Orlicki, R. S. Reiner, A. W. Rudie, *Carbohydr. Polym.* **2012**, *87*, 2488.
- [10] H. Liu, Pengand Sehaqui, P. Tingaut, A. Wichser, K. Oksman, A. P. Mathew, *Cellulose* **2014**, *21*, 449.
- [11] Z. Liu, Y. Jiao, Y. Wang, C. Zhou, Z. Zhang, *Adv. Drug Delivery Rev.* **2008**, *60*, 1650.
- [12] T.-L. Yang, *Int. J. Mol. Sci.* **2011**, *12*, 1936.
- [13] B. Krajewska, *Enzyme Microb. Technol.* **2004**, *35*, 126.
- [14] K. Igarashi, T. Uchihashi, T. Uchiyama, H. Sugimoto, M. Wada, K. Suzuki, S. Sakuda, T. Ando, T. Watanabe, M. Samejima, *Nat. Commun.* **2014**, *5*, 3975.
- [15] J. D. Kittle, C. Wang, C. Qian, Y. Zhang, M. Zhang, M. Roman, J. R. Morris, R. B. Moore, A. R. Esker, *Biomacromolecules* **2012**, *13*, 714.
- [16] J. You, M. Li, B. Ding, X. Wu, C. Li, *Adv. Mater.* **2017**, *29*, 1606895.
- [17] J.-K. Kim, D. H. Kim, S. H. Joo, B. Choi, A. Cha, K. M. Kim, T.-H. Kwon, S. K. Kwak, S. J. Kang, J. Jin, *ACS Nano* **2017**, *11*, 6114.
- [18] V. Zargar, M. Asghari, A. Dashti, *ChemBioEng Rev.* **2015**, *2*, 204.
- [19] M. Rinaudo, *Prog. Polym. Sci.* **2006**, *31*, 603.
- [20] S. Ifuku, M. Nogi, K. Abe, M. Yoshioka, M. Morimoto, H. Saimoto, H. Yano, *Biomacromolecules* **2009**, *10*, 1584.
- [21] R. Minke, J. Blackwell, *J. Mol. Biol.* **1978**, *120*, 167.
- [22] P. Sikorski, R. Hori, M. Wada, *Biomacromolecules* **2009**, *10*, 1100.
- [23] Y. Saito, T. Okano, H. Chanzy, J. Sugiyama, *J. Struct. Biol.* **1995**, *114*, 218.
- [24] M. Rolandi, R. Rolandi, *Adv. Colloid Interface Sci.* **2014**, *207*, 216.
- [25] Y. Tan, S. Hoon, P. A. Guerette, W. Wei, A. Ghadban, A. Hao, Caiand Miserez, J. H. Waite, *Nat. Chem. Biol.* **2015**, *11*, 488.
- [26] R. Cody, N. Davis, J. Lin, D. Shaw, *Biomass* **1990**, *21*, 285.
- [27] G. Vaaje-Kolstad, D. R. Houston, A. H. Riemen, V. G. Eijsink, D. M. van Aalten, *J. Biol. Chem.* **2005**, *280*, 11313.
- [28] H. Pyles, S. Zhang, J. J. De Yoreo, D. Baker, *Nature* **2019**, *571*, 251.
- [29] A. H. Brown, T. R. Walsh, *Carbohydr. Polym.* **2016**, *151*, 916.
- [30] G. Vaaje-Kolstad, B. Westereng, S. J. Horn, Z. Liu, H. Zhai, M. Sørlie, V. G. H. Eijsink, *Science* **2010**, *330*, 219.
- [31] M. Qu, T. Watanabe-Nakayama, S. Sun, K. Umeda, X. Guo, Y. Liu, T. Ando, Q. Yang, *ACS Catal.* **2020**, *10*, 13606.
- [32] G. Usov, Ivanand Nyström, J. Adamcik, S. Handschin, C. Schütz, A. Fall, L. Bergström, R. Mezzenga, *Nat. Commun.* **2015**, *6*, 7564.
- [33] J. D. Goodrich, W. T. Winter, *Biomacromolecules* **2007**, *8*, 252.
- [34] T. Fukuma, B. Reischl, N. Kobayashi, P. Spijker, F. F. Canova, K. Miyazawa, A. S. Foster, *Phys. Rev. B* **2015**, *92*, 155412.
- [35] A. F. R. V. Maurer, *Cellulose* **2013**, *20*, 25.
- [36] A. Baker, W. Helbert, J. Sugiyama, M. Miles, *Biophys. J.* **2000**, *79*, 1139.
- [37] Y. Ogawa, S. Kimura, M. Wada, S. Kuga, *J. Struct. Biol.* **2010**, *171*, 111.
- [38] N. A. Gow, G. W. Gooday, J. D. Russell, M. Wilson, *Carbohydr. Res.* **1987**, *165*, 105.
- [39] T. C. Davidson, R. H. Newman, M. J. Ryan, *Carbohydr. Res.* **2004**, *339*, 2889.
- [40] A. P. Heiner, L. Kuutti, O. Teleman, *Carbohydr. Res.* **1998**, *306*, 205.
- [41] T. Fukuma, R. Garcia, *ACS Nano* **2018**, *12*, 11785.

- [42] T. Fukuma, Y. Ueda, S. Yoshioka, H. Asakawa, *Phys. Rev. Lett.* **2010**, *104*, 016101.
- [43] K. Miyata, J. Tracey, K. Miyazawa, V. Haapasilta, P. Spijker, Y. Kawagoe, A. S. Foster, K. Tsukamoto, T. Fukuma, *Nano Lett.* **2017**, *17*, 4083.
- [44] H. Söngen, B. Reischl, K. Miyata, R. Bechstein, P. Raiteri, A. L. Rohl, J. D. Gale, T. Fukuma, A. Kühnle, *Phys. Rev. Lett.* **2018**, *120*, 116101.
- [45] D. Martin-Jimenez, E. Chacon, P. Tarazona, R. Garcia, *Nat. Commun.* **2016**, *7*, 12164.
- [46] H. Asakawa, S. Yoshioka, K.-i. Nishimura, T. Fukuma, *ACS Nano* **2012**, *6*, 9013.
- [47] M. R. Uhlig, D. Martin-Jimenez, R. Garcia, *Nat. Commun.* **2019**, *10*, 2606.
- [48] I. Schlesinger, U. Sivan, *J. Am. Chem. Soc.* **2018**, *140*, 10473.
- [49] K. Umeda, L. Zivanovic, K. Kobayashi, J. Ritala, H. Kominami, P. Spijker, A. S. Foster, H. Yamada, *Nat. Commun.* **2017**, *8*, 2111.
- [50] K. Kimura, S. Ido, N. Oyabu, K. Kobayashi, Y. Hirata, T. Imai, H. Yamada, *J. Chem. Phys.* **2010**, *132*, 194705.
- [51] K. Kuchuk, U. Sivan, *Nano Lett.* **2018**, *18*, 2733.
- [52] T. Ikarashi, T. Yoshino, N. Nakajima, K. Miyata, K. Miyazawa, Y. Morais Jaques, A. S. Foster, M. Uno, C. Takatoh, T. Fukuma, *ACS Appl. Nano Mater.* **2021**, *4*, 71.
- [53] C.-W. Yang, K. Miyazawa, T. Fukuma, K. Miyata, I.-S. Hwang, *Phys. Chem. Chem. Phys.* **2018**, *20*, 23522.
- [54] J. F. Matthews, C. E. Skopec, P. E. Mason, P. Zuccato, R. W. Torget, J. Sugiyama, M. E. Himmel, J. W. Brady, *Carbohydr. Res.* **2006**, *341*, 138.
- [55] K. Miyazawa, J. Tracey, B. Reischl, P. Spijker, A. S. Foster, A. L. Rohl, T. Fukuma, *Nanoscale* **2020**, *12*, 12856.
- [56] E. Nakouzi, A. G. Stack, S. Kerisit, B. A. Legg, C. J. Mundy, G. K. Schenter, J. Chun, J. J. De Yoreo, *J. Phys. Chem. C* **2021**, *125*, 1282.
- [57] W. J. Lee, A. J. Clancy, E. Kontturi, A. Bismarck, M. S. P. Shaffer, *ACS Appl. Mater. Interfaces* **2016**, *8*, 31500.
- [58] C. H. Lemke, R. Y. Dong, C. A. Michal, W. Y. Hamad, *Cellulose* **2012**, *19*, 1619.
- [59] Q. Wu, W. shou Miao, Y. du Zhang, H. jun Gao, D. Hui, *Nano-technol. Rev.* **2020**, *9*, 259.
- [60] Y. Fan, H. Fukuzumi, T. Saito, A. Isogai, *Int. J. Biol. Macromol.* **2012**, *50*, 69.
- [61] Y. Ogawa, R. Hori, U.-J. Kim, M. Wada, *Carbohydr. Polym.* **2011**, *83*, 1213.
- [62] R. Sinko, S. Keten, *Appl. Phys. Lett.* **2014**, *105*, 243702.
- [63] J. R. Capadona, K. Shanmuganathan, D. J. Tyler, S. J. Rowan, C. Weder, *Science* **2008**, *319*, 1370.
- [64] A. A. Skelton, T. Liang, T. R. Walsh, *ACS Appl. Mater. Interfaces* **2009**, *1*, 1482.
- [65] Y. He, Y. Chang, J. C. Hower, J. Zheng, S. Chen, S. Jiang, *Phys. Chem. Chem. Phys.* **2008**, *10*, 5539.
- [66] L. Petridis, J. C. Smith, *Nat. Rev. Chem.* **2018**, *2*, 382.
- [67] T.-D. Nguyen, K. E. Shopsowitz, M. J. MacLachlan, *Chem. - Eur. J.* **2013**, *19*, 15148.
- [68] T. Fukuma, M. Kimura, K. Kobayashi, K. Matsushige, H. Yamada, *Rev. Sci. Instrum.* **2005**, *76*, 053704.
- [69] J. L. Hutter, J. Bechhoefer, *Rev. Sci. Instrum.* **1993**, *64*, 1868.
- [70] B. J. Albers, T. C. Schwendemann, M. Z. Baykara, N. Pilet, M. Liebmann, E. I. Altman, U. D. Schwarz, *Nat. Nanotechnol.* **2009**, *4*, 307.
- [71] T. Fukuma, *Sci. Technol. Adv. Mater.* **2010**, *11*, 033003.
- [72] B. Reischl, P. Raiteri, J. D. Gale, A. L. Rohl, *J. Phys. Chem. C* **2019**, *123*, 14985.
- [73] L. Martínez, R. Andrade, E. G. Birgin, J. M. Martínez, *J. Comput. Chem.* **2009**, *30*, 2157.
- [74] S. Plimpton, *J. Comput. Phys.* **1995**, *117*, 1.
- [75] A. I. Jewett, D. Stelter, J. Lambert, S. M. Saladi, O. M. Roscioni, M. Ricci, L. Autin, M. Maritan, S. M. Bashusqeh, T. Keyes, R. T. Dame, J.-E. Shea, G. J. Jensen, D. S. Goodsell, *J. Mol. Biol.* **2021**, *433*, 166841.
- [76] G. T. Beckham, M. F. Crowley, *J. Phys. Chem. B* **2011**, *115*, 4516.
- [77] R. Hockney, J. W. Eastwood, *Computer Simulation Using Particles*, McGraw-Hill, New York **1981**.
- [78] N. Michaud-Agrawal, E. J. Denning, T. B. Woolf, O. Beckstein, *J. Comput. Chem.* **2011**, *32*, 2319.
- [79] R. J. Gowers, M. Linke, J. Barnoud, T. J. E. Reddy, M. N. Melo, S. L. Seyler, J. Domański, D. L. Dotson, S. Buchoux, I. M. Kenney, O. Beckstein, in *Proc. of the 15th Python in Science Conf.*, (Eds: S. Benthall, S. Rostrup), SciPy, Austin, TX **2016**, pp. 98–105.